Induction heating-based low-frequency alternating magnetic field: High potential of ferromagnetic composites for medical applications

Ziyin Xiang, Benjamin Ducharne, Nellie Della Schiava, Jean-Fabien Capsal, Pierre-Jean Cottinet, Gildas Coativy, Patrick Lermusiaux, Minh-Quyen Le

Version of Record: https://www.sciencedirect.com/science/article/pii/S0264127519302412
Manuscript_1e6e57e80f651671aab37d74f7606377

Induction Heating-based Low-Frequency Alternating Magnetic Field: High Potential of Ferromagnetic Composites for Medical Applications

Ziyin Xiang[1], Benjamin Ducharne[1], Nellie Della Schiava[1,2], Jean-Fabien Capsal[1], Pierre-Jean Cottinet[1], Gildas Coativy[1], Patrick Lermusiaux[2,3], Minh Quyen Le[1*].

[1]Univ. Lyon, INSA-Lyon, LGEF, EA682, F-69621, VILLEURBANNE, France
[2]Groupement Hospitalier Edouard Herriot, 69003 Lyon, France
[3]Université Claude Bernard Lyon 1 (Univ Lyon), 8 Avenue Rockefeller Lyon, F-69621 Villeurbanne, France

* Corresponding author: minh-quyen.le@insa-lyon.fr

Abstract: This study focusses on a low-frequency induction heating (LFIH) effect in a thermoplastic polymer (acrylonitrile butadiene styrene, ABS) filled with iron oxide magnetic particles. The LFIH effect in such ferromagnetic composites appears as soon as the sample is exposed to an alternating magnetic excitation field and is mainly due to the so-called "microscopic" eddy currents linked to the motions of the magnetic domain wall. To generate an AC magnetic field with significant amplitude under a low-frequency range of a few thousand Hz, a specific test bench has been designed using a rotating motor and strong permanent magnets. Theoretical hysteresis modeling, together with thermal transfer based Comsol simulation and experimental tests, demonstrated the feasibility of significantly increasing the temperature of a magnetic composite through a simple induction heating effect. To better highlight such an effect, a comparison with conductive but non-ferromagnetic samples was performed. As opposed to the ferromagnetic composite, its conductive counterpart exhibited a very weak response to the magnetic field excitation, and no temperature effect was achieved. This observation can be explained by "microscopic" eddy currents (i.e., the fact that domain wall motions are predominant mechanisms under low frequency), leading to local temperature variations inside the ferromagnetic particles. These preliminary results seem to be promising, and this effect could be exploited in a medical application, especially for treatment of superficial venous insufficiency, where local heating remains a true challenge. As normal tissues and muscles are conductive, it is necessary to bring the heat "where it is needed". We believe that LFIH would be able to destroy varicose veins without damaging the neighboring tissues.

Keywords: Ferromagnetic composites, hysteresis loss, microscopic eddy current, low-frequency induction heating, thermal transfer modeling, treatment of superficial venous insufficiency, medical applications.

I INTRODUCTION

Ferromagnetic composites with magnetic particles embedded in a polymer matrix are currently of great interest from a scientific viewpoint. Incorporation of particles, fibers or nanomaterial reinforcements into polymers permit the fabrication of polymer matrix composites, which can be characterized by high mechanical performance and excellent functionality [1]. Particle reinforcements have been developed to improve mechanical properties: enhance tensile/storage modulus by adding glass beads [2], iron or copper particles [3], and enhance wear resistance by adding aluminum and aluminum oxide (Al_2O_3) [4]. Combining ferromagnetic particles with a polymer matrix creates an opportunity for potential enhancements in both mechanical and magnetic properties. Among applications based on ferromagnetic composites, induction heating is currently one of the hot topics related to numerous fields, such as self-healing polymers, thermal welding, and magnetic hyperthermia. The main benefits over other heating methods include the selectivity of the heated area, the fast response time, and good efficiency [5].

The induction heating effect of ferromagnetic materials, which appears when such materials are exposed to an alternating (AC) magnetic field, is based on the so-called "macroscopic" eddy currents and "microscopic" eddy currents (i.e., hysteresis loss). The frequency dependence of these two contributions differs in that: The so-called "microscopic" eddy currents originate from the interactions between the walls of the magnetic domains and the microstructure during the magnetization of the sample [6]; whereas the so-called "macroscopic" eddy currents are linked to the diffusion equation [7] of the magnetic field and are strongly dependent on the physical properties of the material (e.g., conductivity and permeability).

In the case of low-frequency induction heating (LFIH), only the so-called "microscopic" eddy currents exist inside the ferromagnetic composite, and this paper will demonstrate such an effect through experimental investigation. Induction heating phenomena were highlighted and validated via both empirical tests and thermal transfer modeling based COMSOL simulation. The final goal of this research is aimed at employing the developed composite for medical purposes, particularly in the minimally invasive endovascular treatment of

superficial venous insufficiency. The new concept proposed here is to introduce a biocompatible magnetic composite into an abnormal vein and heat it under high-temperature thanks to an external AC magnetic field. Due to the dominant hysteresis loss, only particles under magnetic excitation would be active, making it possible to locally heat the pathologic vein without damaging the surrounding healthy tissue.

Historical treatment of superficial venous insufficiency is stripping of the incontinent vein with or without phlebotomy of varicose veins. In the last few years, several minimally invasive, endovenous, procedures have been developed . These endovenous thermal ablation (EVTA) consists of endovenous laser ablation (EVLA), endovenous steam ablation (EVSA), and radiofrequency ablation (RFA). Compared to classical surgery, minimally invasive treatment highly benefits patients, with less pain and overall easier recovery [8]. Of all the thermal ablation practices, EVLA is the most frequently used technique, followed by RFA, whereas EVSA is a new technique that has not yet been extensively studied. To effectively treat incontinent veins, most of the endovenous ablation need to reach a temperature of 120°C [9], except for RFA procedures performed with the VNUS® Closure Plus system [10], which heats local tissue to only 85–90°C at the site of direct contact. This lower maximal temperature probably results in less postoperative pain than EVLA. However, the main drawback of RFA is related to its instructions for use. For instance, it is impossible for segmental RFA (performed by VNUS® Closure Fast which is currently the most popular method) to treat veins with a length smaller than 7 cm [9] or veins with a diameter greater than around 15 mm. Furthermore, this technique does not allow for varying the energy delivered, as opposed to EVLA where the total amount of supplied energy per centimeter can be changed by simply adjusting the pullback speed/power. For small veins, only 20 J/cm is used, whereas higher energy (i.e., 60 J/cm) is needed when treating large veins. Moreover, all the endovenous techniques exhibits some serious weakness. Indeed, the fact of implanting guidewire to introduce thermal probes induces a risk of vessel perforation, especially in very tortuous veins [9]. Another disadvantage in these techniques is the need to perform an injection of bicarbonate serum in the subcutaneous tissues between the vein and the skin, called swelling technique, in order to prevent the risk of burns of these tissues. This step of the surgical intervention is tricky and very time-consuming.

In this paper, we propose an alternative endovenous approach to treat superficial venous insufficiency based on LFIH mechanism which is similar to technique of endovenous thermal ablation. The purpose here is not to make a competition to the current EVTA methods, but rather to show some further benefits induced by LFIH as well as to demonstrate a feasibility to heat the ferromagnetic composite by using an alternative low-frequency magnetic field. Simulation and experimental results are very promising, showing high potential of the proposed approach for medical application especially in thermal treatment of superficial venous insufficiency. The LFIH principle is related to the so-called microscopic eddy current, which appears inside the magnetic particles when excited by an alternative magnetic source. As this source is implemented outside the patient who has no physical connection to the composite introducing into the vessel, LFIH leads to a much easier procedure relative to existing techniques. However, the distance between the source and heated target should be carefully controlled as it can greatly affect the magnetic intensity. Another advantage of LFIH is its “selective” heat that only occurs on ferromagnetic material, thereby making it possible not to burn or hurt neighboring tissues. Consequently, the LFIH method will probably be safer for patients and can avoid some postoperative complications, such as nerve damage, skin burns and bleeding (which can occur with EVLA) [11]. Additionally, with LFIH we might not need to perform swelling technique, allowing to considerably reduce the surgical time as well as the global costs. Moreover, this technique uses ferromagnetic composites involving ABS polymer matrix doped with magnetic filler, so it has high potential to be combined with 3D printing technology [12,13]. Adapting 3D-printing to additive manufacturing creates the possibility of achieving smart material with various special shapes and sizes suitable for multiple diameter and length of veins, which will be one of our top priorities for future research. Finally, a linear dependence of magnetic intensity on the rotational motor frequency provides an easy way for LFIH to vary energy delivery during a medical procedure, which is impossible in the case of RFA.

In an era of health technology assessment and cost-effectiveness analyses, treatment-related costs become increasingly important. EVLA is the least expensive endothermal treatment, and the cheapest laser disposables cost approximately 120 Euros [9]. Throughout the treatment, patients must wear special goggles or eyeglasses to protect their eyes from the laser light. The RFA Procedure-related costs are higher due to the higher cost of the catheter [14]. Generally, the additional cost of $110–$220 per patient is mainly related to the cost of consumables [15]. Although it is too early to estimate the total costs of using LFIH, we believe that this method

will be cost-effective due to cheap commercially available materials, such as thermoplastic (ABS) and magnetic powder (iron oxide), together with its simple fabrication process.

In conclusion, the proposed approach, based on the LFIH effect, can be an interesting solution for endovenous thermal ablation, which might enable a safer and easier procedure than EVLA; thereby lowering costs and increase applicability compared to RFA.

II MANUFACTURING OF MATERIAL

Since the final goal of this work was medical applications, the magnetically reinforced material should be biocompatible. Among several magnetic particles, iron oxide (Fe_3O_4) seems to be a promising candidate thanks to its confirmed biocompatibility [16]. Also, this material has been widely studied in recent years due to its interesting magnetic properties, making it potentially interesting for numerous applications [17]. Regarding the polymer matrix, the thermoplastic ABS (acrylonitrile butadiene styrene) was considered a suitable choice due to its widespread commercial use, particularly in injection molding and 3D printing [18,19].

The elaboration procedure of the ferromagnetic composite is illustrated in Figure 1. First, ABS granules were dissolved in acetone with vigorous stirring at room temperature during 2 h until the ABS went completely into solution. Second, a spherical powder (5 µm in diameter) of the Fe_3O_4 (SIGMA-ALDRICH) was added, and stirring was continued for 1 h to achieve a perfectly homogeneous solution (Figure 1 (a) –A). The volume content of Fe_3O_4 in the ABS varied from 3% to 17%, which was sufficiently small to avoid the percolation threshold of the composite. Considering that the particle distribution was homogeneous, each particle was assumed to be electrically insulated. Such electrical insulation will prevent the formation of a macroscopic eddy current, and consequently, the ferromagnetic losses will be limited to the domain wall motions, resulting in microscopic eddy currents and a local induction heating effect.

a) b)

Figure 1. a) Fabrication process of the composites. b) Three groups of samples (from left to right): ferromagnetic composites, two conductive composites filled with copper and carbon black, and pure ABS.

With the aim of improving the dispersion of the iron powder in the ABS matrix, the solution was scattered by ultrasound treatment (Hielscher Ultrasonic Processor UP400S) with powerful impulsion during a few minutes (Figure 1(a)-B). Subsequently, precipitation of the solution in ethanol was carried out within 30 min to freeze the composite in a good dispersion state, avoiding sedimentation of the particles in the polymer solution. Next, the obtained solution was transferred into an evaporating dish, and the collected supernatant liquid was withdrawn (Figure 1(a)-C). The sample was then put in the oven (Memmert Typ: V0 400) at 56°C (corresponding to the acetone volatilization temperature) for 2h to totally evaporate the solvent (Figure 1(a)-D). The powdered composite was then slowly hot pressed (Figure 1(a)-E) at 220°C under a pressure of 1300 Psi in a hydraulic press (CARVER 3851CE). Such a temperature is closed to the melting temperature of ABS thermoplastic (~ 210°- 230°) so that to ensure perfectly compact homogenous block. Finally, the quality of the fabrication process can be verified by measuring the density of the sample and comparing it to the theoretical value obtained by the mixture rule as described Eq. (1). It should be ensured that there are no air bubbles inside the sample because such micro “holes” can significantly alter the magnetic line.

$$\rho_{composite} = (1 - x)\rho_{ABS} + x\rho_{particle} \quad (1)$$

where x is the volume fraction of the particle; $\rho_{composite}$, ρ_{ABS} (1.05 g·cm^{-3}), and $\rho_{partile}$ (5.17 g·cm^{-3}) denote the volumic masses of the composite, the ABS thermoplastic, and the iron oxide microparticle, respectively.

All samples were a rectangular shape with dimensions of 60 × 14 × 4 mm, as illustrated in Figure 1(b). Three groups were performed, comprising the ferromagnetic composite reinforced by Fe_3O_4 particles, two conductive composites respectively filled with 15% vol. of copper and 5% vol. of carbon black, and the pure ABS sample.

III HYSTERESIS MODEL BASED LUMP MODEL

Many articles discuss the magnetic behavior of Fe_3O_4 nanoparticles [20–22]. It is demonstrated that particles larger than 15 nm diameter exhibit a ferrimagnetic behavior. For such particles, even if the experimental process is complex, a classic quasi-static hysteresis cycle signature can be plotted. Usually, coercive field values are close to 30,000 A/m (H_c), remnant inductions (B_r) close to 0.04 T, and saturation inductions (B_{sat}) slightly higher than 0.1 T [23]. At this size, the particle is supposed to be large enough, to be organized into a large number of magnetic domains. The hysteretic behavior comes from the energy required to modify the domains' shapes and organization.

In the first results coming (microscopy), we noticed a homogeneous distribution of the particles; small agglomerates can also be observed. As the particles (Sigma-Aldrich) used in the composite are spherical, and their diameters are approximately 5 µm, it is possible to assimilate its magnetic behavior as barely similar to a macroscopic bulk ferrite [24]. Figure 2 gives a schematic illustration of the magnetic composite.

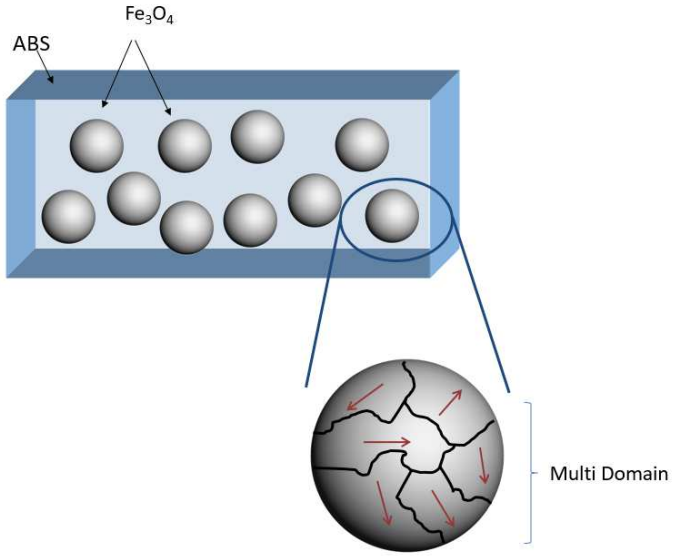

Figure 2. Schematic illustration of the magnetic composite.

Bulk ferrites are ceramic materials made by mixing large proportions of iron oxide and additional metallic elements, such as barium, manganese, nickel, and zinc. One notable characteristic of ferrites comes from their ability to be both electrically non-conductive and ferromagnetic (i.e., ferrites can be magnetized and attracted to permanent magnets). Soft ferrites can have relatively low coercive fields. Their natural weak electrical conductivity forbids macroscopic eddy currents even under large frequency levels, and in such ceramic compounds, the magnetic skin effect is always absent. Thus, bulk ferrites are particularly useful for applications where magnetic conversions are required under large frequency solicitations (high-frequency inductors and transformers, switched-mode power supplies, loop stick antennas, microwave components, and so on).

Even if macroscopic eddy currents cannot develop inside bulk ferrites, their magnetic behavior is still frequency dependent. This dependence comes from the amplitude and density of microscopic eddy currents (linked to the magnetic domain wall motions), which vary versus the magnetic excitation dynamic. By plotting a ferrite hysteresis area versus frequency (Figure 3a), low variations can be observed from very weak frequency levels to a cut-off frequency value called the quasi-static threshold. Once this threshold frequency is overpassed, the

hysteresis area roughly increases meaning that, to be magnetized, larger energy is required. The hysteresis area is supposed to reach a maximum for extremely high-frequency values, then to sharply decrease, but set-up limitations never allowed experimental confirmation of this behavior. Based on the result of Figure 3a, the normalized hysteresis power can be deduced as described in Figure 3b.

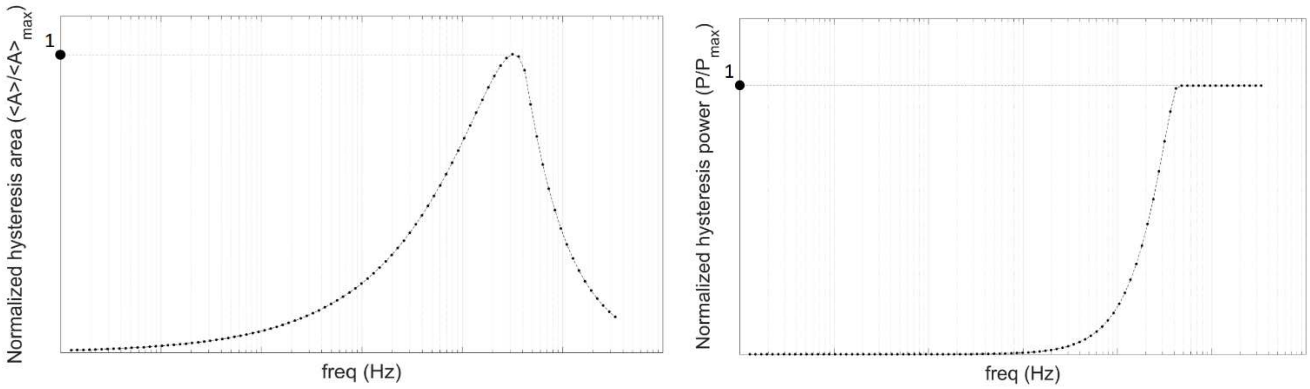

a) b)

Figure 3. Logarithmic frequency dependence of a) normalized hysteresis area and b) normalized hysteresis power for a ferrite bulk (simulation result).

As commented already, the weak conductivity of ferrite ceramics forbids the development of macroscopic eddy currents. This absence means there is no magnetic skin effect and a homogeneous distribution of the magnetic fields (H and B). From the simulation point of view, this means that space discretization schemes are not necessary and lump approaches will be accurate enough. The best results for the simulation of a ferrite hysteretic behavior using the lump model is the sum of two contributions: A quasi-static contribution, frequency independent and unique below quasi-static threshold; and a dynamic contribution, a product of a dissipative constant ρ to the time derivation of the induction field dB/dt.

Different options are available in the literature for a phenomenological simulation of the quasi-static contribution [25]. Among all, the Preisach and the Jiles-Atherton (J-A) models are the most popular [26–30]. Both exhibit the property of being reversible. H or B can be used as the model input according to the experimental situation simulated. The Preisach model seems a little more accurate, but the intrinsic congruency issue and memory management are major limitations. The J-A model relies on physical fundaments; each of the five parameters has a physical meaning. On the one hand, such a physical-based approach is certainly a major positive aspect of the model and helps the user establish physical interpretations of their simulation results. On the other hand, the accommodation issue and the fastidious and hazardous quest for the perfect parameter combination reduce the convenience of this model.

The simulation scheme we have been working with relies on the following equation:

$$\rho.\frac{dB(t)}{dt} = H_{surf}(t) - f^{-1}_{quasi-static}(B(t)) \tag{2}$$

Here, ρ is the dissipative constant defined previously (ρ depends on the nature and geometry of the sample), H_{surf} is the surface tangent magnetic excitation field, and f^{-1} the inverse quasi-static contribution function [6,31–33]. It is worth noting that each term of this equation acts as an H equivalent contribution.

Eq. (2) has been used with success many times for the simulation of non-conductive magnetic materials [34], but to go forward with our composite simulation process using this equation, several issues needed to be addressed. One of them is the determination of the quasi-static threshold. This will indirectly set the value of ρ. A combination of the f^{-1} consistent parameter with the experimental hysteresis values given at the beginning of this part (H_c, B_r, and B_{sat}) will also have to be set. After several tests, due to its physical fundaments, a B imposed Jiles-Atherton model has finally been chosen for the expression of f^{-1}.

Our experimental setup and the magnetic circuit geometry are very far from the ideal case of standard magnetic characterization setups (e.g., its ring shape [35], Epstein bench [36,37], single sheet tester [38,39]). It is consequently impossible to obtain accurate and reproducible sample magnetic signatures from this experimental

setup. To solve this, one option we have is to design a sample of geometry fitting the standard characterization norms (by instance, like a ring shape) and surrounding it with excitation coils. But the extreme amplitude and frequency of magnetic excitation provided by the combination permanent magnet/electric drill will be very complex to reach with surrounding coils. Another option is to go through indirect thermic experimental/simulation results and to fit the simulated hysteresis area with the amplitude of the thermal flux sources.

The thermal simulation recreates the experimental situation through finite element discretization. Exchanges are considered between the magnetic composite and the surrounding environment. The magnetic sample is characterized by the given thermal conductivity and capacity. Magnetic heating power (MHP) simulating the thermal behavior of the Fe_3O_4 particles are considered inside the magnetic composite. The amplitude of this source is set when the composite average temperature time variations match the experimental variations. More details about the simulation based thermal transfer model are later reported in subsection IV.3. It will be shown that the evolution of the magnetic heating energy remains relatively constant (around 20–25 kJ.m^{-3}) regardless of the frequency. As this energy can be assimilated to the magnetic hysteresis area, this observation means that even if the maximum frequency tested is relatively high (2300 Hz); the quasi-static threshold is still in a higher range than this. Using the obtained information relating to H_c, B_r, B_{sat}, and hysteresis area, a hysteresis cycle shape shown in Figure 4, can be determined.

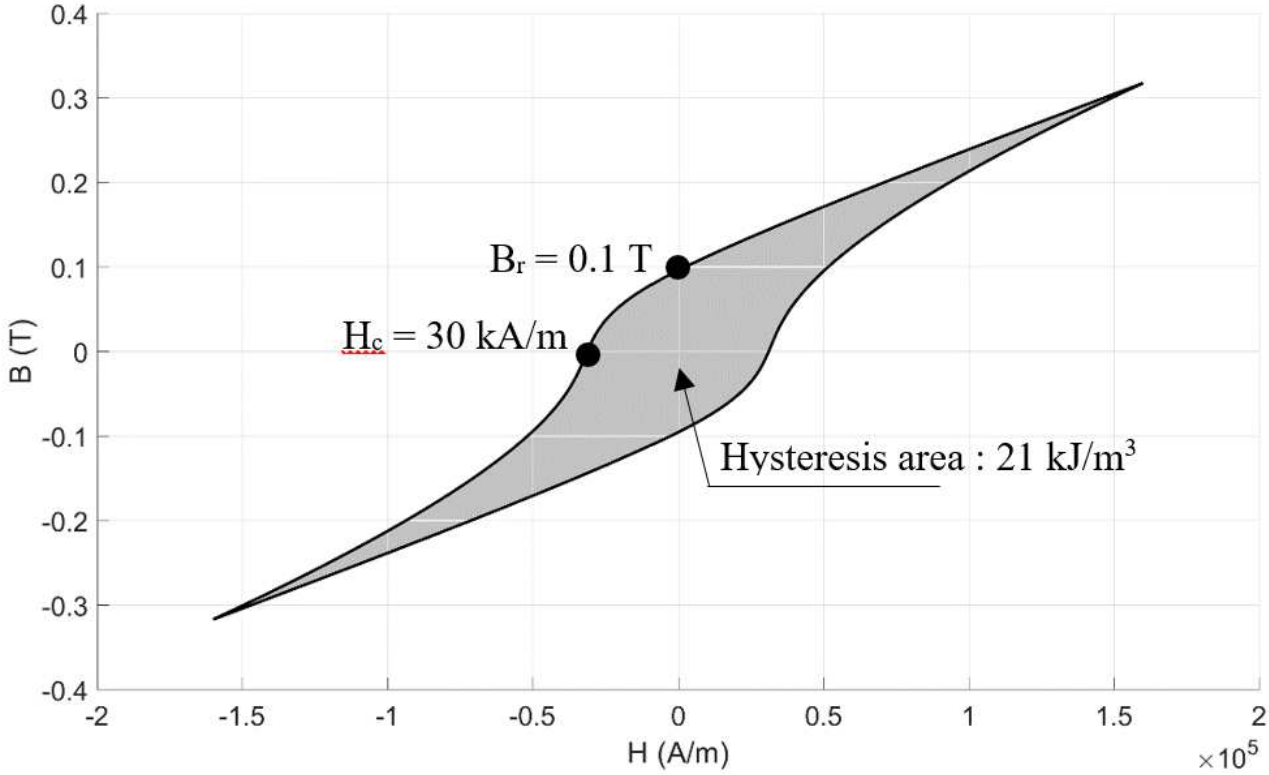

Figure 4. Hysteresis cycle-based modeling result.

To reach a hysteresis area matching the thermal simulation results, the induction levels have to be slightly higher than the expected levels. This improvement in the magnetic behavior could be explained from the geometrical scaling differences between the particles and the agglomerates.

J-A's model optimized parameters were used for the simulation of the hysteresis cycle and are shown in Figure 4 and Table 1.

The Langevin function of Eq. (3) is used as an analytical expression of the anhysteretic curve:

$$M_{anh}(H_{surf}) = M_s.\tan^{-1}\left(\frac{H_{surf}}{a}\right) \tag{3}$$

By mixing thermal and magnetic simulation results, we succeed in recreating the magnetic signature of the particle distribution. We notice that the current working frequencies are below the quasi-static threshold,

meaning that the current working frequencies are still in the weak variation part of the energy versus frequency curve. This also means that large improvements in the temperature variations can be obtained by working in the higher frequency ranges.

Table 1. J-A-s model optimized parameters.

J-A model parameters	Optimized values
a (A/m)	$5.0\ 10^4$
α	0.8
k (A/m)	$1.2\ 10^5$
c	0.4
Ms (A/m)	$8.5\ 10^4$

Finally, a compromise will have to be done between frequency limitations due to the surrounding tissue that should not be burnt and the increasing of the working frequency, which is necessary to improve the amount of magnetic energy converted (i.e., the energy required to reach the targeted temperature).

IV INDUCTION HEATING EFFECT: RESULTS AND DISCUSSIONS

IV.1 Experimental setup

For the validation of the induction heating effect, a specific experimental test-bench was developed (Figure 5). To generate a significant AC magnetic field excitation, a 70mm-diameter magnetic inductor was assembled to a DC drill motor that can generate variable speed. The magnetic inductor consisted of eight cubic permanent magnets with 10 mm edge lengths. The pole distribution of the eight magnets was alternatively south and north, as shown in Figure 6 a), enabling the production of a sinusoidal magnetic excitation whose frequency was four times higher than the one driven by the DC motor. The following equation enables us to deduce the relationship between the motor's velocity (denoted v (RPM)) and the frequency (denoted $f(Hz)$) of the magnetic field excitation:

$$f = \frac{v}{60} \times 4 = \frac{v}{15} \tag{4}$$

Based on the Fourier transformer of the measured magnetic field as displayed in Figure 6b), it is possible to precisely determine its frequency. An experimental measure of the motor's velocity together with the spectra analysis of Figure 6b) allowed us to confirm the expression of Eq (3). Furthermore, the result revealed that the magnetic excitation signal is purely sinusoidal as parasite harmonics are negligible compared to the principal harmonics. Finally, the current test bench can drive a maximum rotating speed of 35 kRPM, leading to the highest frequency of 2300 Hz for the magnetic field. The sample was fixed on the removable support, making it possible to vary the distance to the magnetic inductor. Two thermal couples were coated on the sample via an adhesive; one allowed us to measure the temperature of heat area corresponding to magnet's passage, and the other used to determine the temperature of the sample's center. Both data sets were recorded in real time through a DEWE card (Krypton). To obtain a more intuitive temperature image, a thermal camera (Optris Xi400) was used during the experiment.

To better highlight the induction heating effect of the proposed ferromagnetic composites, a comparison with respect to conductive but non-ferromagnetic samples (e.g., carbon black or copper) was performed based on the thermal images of Figure 7. As opposed to the ferromagnetic composite, the conductive sample exhibited a very weak response to the magnetic field excitation, and no temperature effect was achieved. This observation was explained by the "microscopic" eddy-current consideration (i.e., domain wall motions were the predominant mechanisms under low frequency), leading to local temperature variations inside the ferromagnetic particles. Finally, experimental results revealed that the frequency dependence of the hysteresis losses only appeared through the ferromagnetic composite, but no reaction was observed on the conductive composites. Similar conclusions have also been reported in [40]. It is interesting to note that the temperature at the center of the ferromagnetic composite (Figure 7a) is lower compared to those at the two sides. This result was consistent with the circular design of the magnetic inductor where the magnetic field was stronger at the periphery (position of 8 permanent magnets) than the one at the center (containing no magnet as shown in Figure 6a).

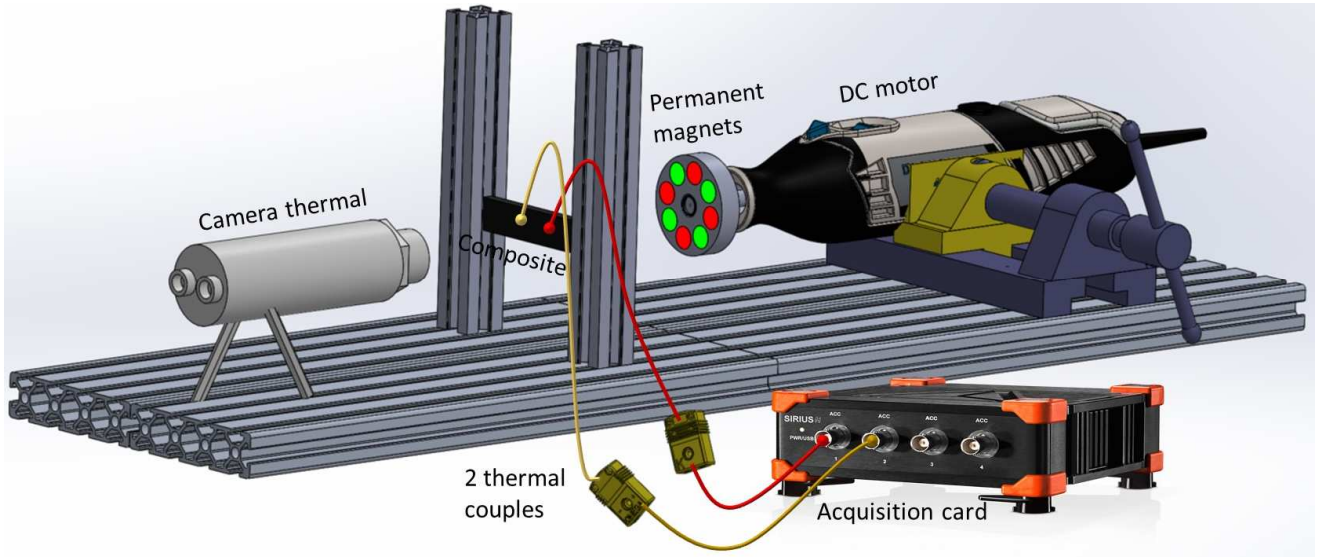

Figure 5. Experimental setup of the induction heating effect.

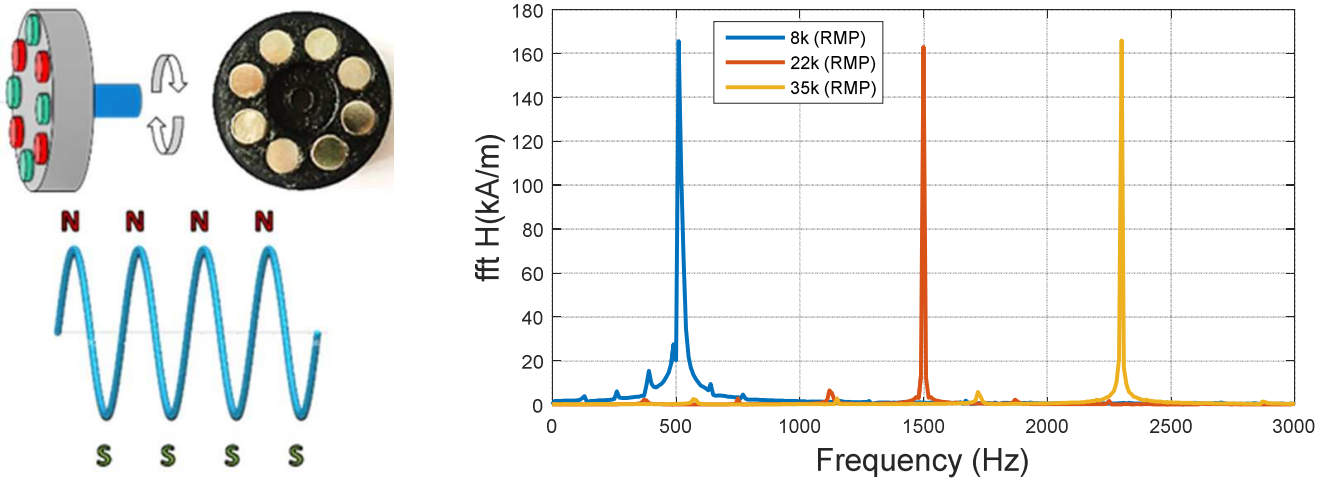

a) b)

Figure 6. a) Design of the magnetic inductor with eight permanent magnets. b) FFT spectra of magnetic field

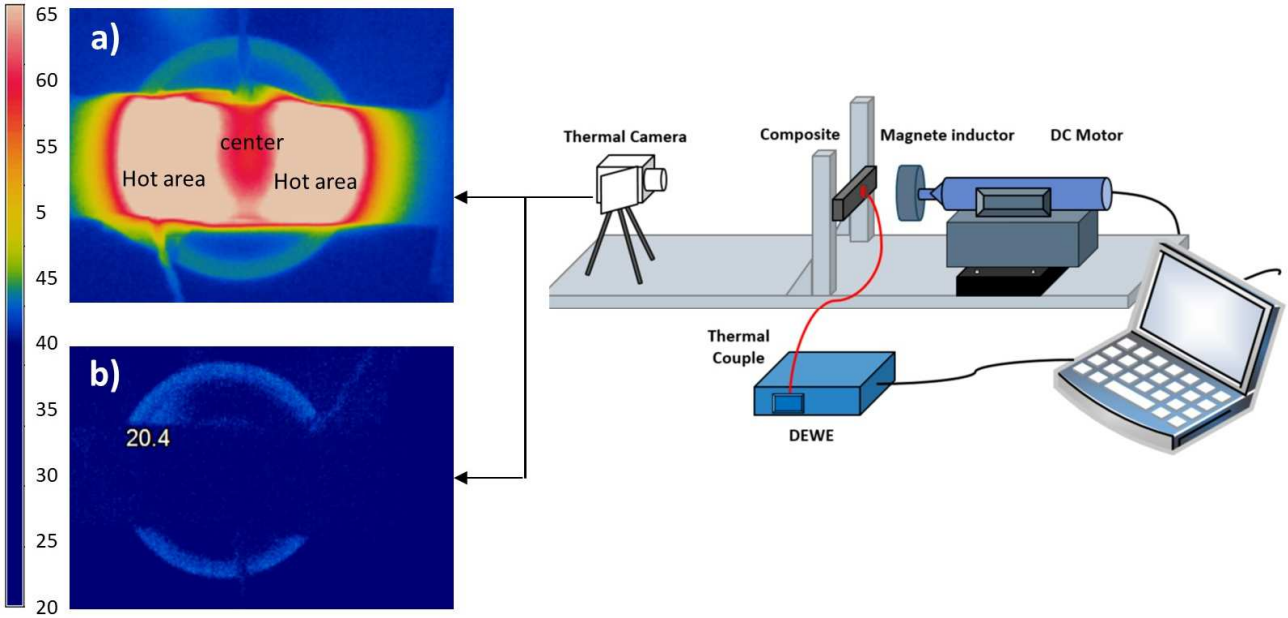

Figure 7. LFIH observation under 2.3 kHz AC magnetic field excitation. a) Ferromagnetic composite with17% vol. of iron oxide. b) conductive composite with 15% of copper oxide.

IV.2 Experimental results

In this study, we discuss the influence of three relevant parameters including fraction content of fillers, frequency, and strength of the magnetic fields on the LFIH effect of ferromagnetic composite. In each analysis, for a better assessment and for an easier understanding, one parameter is varying whereas the two other are fixed and set to be maximum in order to achieve the most optimal condition. For instance, when the volume fraction is changing, the motor is tuned at a full speed (i.e. 35 kRPM) and the distance between the sample and the inductor is as closed as possible in order achieve an alternative field with maximum strength and frequency. Similar approach is applied to the other analyses where the frequency or the amplitude of magnetic source is fixed, sample with highest filler fraction (i.e. 17% vol.) is used. Indeed, based on experimental result that will be shown below, this composite leads to the best induction heating response.

Figure 8a) displays the time evolution in temperature of ferromagnetic composites elaborated with different volume concentrations of 0%, 3%, 6%, 10%, 14%, and 17%. As expected, the temperature remained constant for the pure ABS thermoplastic, whereas this increases for samples with higher magnetic powder content. Indeed, polymer filled with sufficient ferromagnetic particles led to substantially improved permeability, as well as hysteresis losses, giving rise to a drastically increased magnetic power density and therefore, boosting the induction heating effect. Figure 8 b) illustrates the temperature in steady state versus volume fraction of the composite, together with the normalized temperature change ($T_{normalized}$) that can be calculated by:

$$T_{normalized} = \frac{T - T_{ambiant}}{T_{17\%} - T_{ambiant}} \tag{5}$$

where T, $T_{17\%}$ denotes the final temperature of a given sample and the 17% sample, $T_{ambiant}$ was the ambient temperature. The result of Figure 8 b) allowed us to confirm the quasi-linear behavior of the temperature variation as a function of the particle content. Consequently, increasing the magnetic concentration seems to be an easy way to considerably enhance the induction heating performance. Nonetheless, particle percentage should be limited to avoid heterogeneity and percolation threshold that can occur at high filler content (i.e., more than 20% vol.) [41].

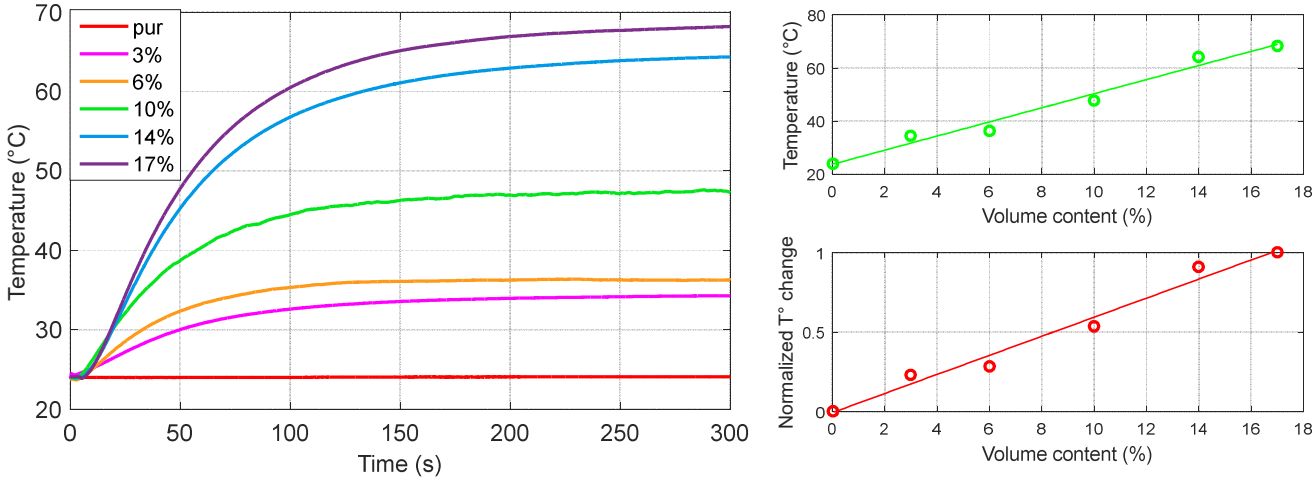

Figure 8. a) Evolution of the temperature with time at different particle fraction. b) Maximum temperature and normalized relative temperature change versus volume fraction concentration.

Figure 9a shows the rise in temperature of the composite with 17% vol. iron oxide filler for several DC motor speed from 5 to 35 kRPM, resulting in variation of the magnetic frequency from 300 to 2300 Hz (cf. Eq. (4)). The results demonstrate a significant temperature increase of the ferromagnetic samples when they were exposed to an alternating magnetic field. As expected, the heating effect was found to be greatly dependent on the frequency. For instance, under the highest frequency of 2300 Hz, the temperature in steady state rose up to 65°C, whereas only 30°C was attained in the case of 300 Hz. This effect can be explained by the fact that the ferromagnetic particles convert the energy of the AC magnetic field into heat based on the physical mechanisms

of the so-called "microscopic" eddy currents. Obviously, the transformation efficiency is strongly depended on the frequency of the external field. The heating experiments confirmed the feasibility to create a hysteresis loss by an electromagnetic field of low frequency using polymers filled with micro-sized magnetic particles.

Based on the result of Figure 9b, a simple linear regression can be used to fit well the experimental data comprising heating temperature versus magnetic frequency. Such a relationship was modeled in accordance with the linear predictor function whose rising slope was estimated to be approximately 1°C/60 Hz. To reach the maximum temperature required for the treatment of superficial venous insufficiency (i.e., 120°C [9]), it was essential to excite the composite with a magnetic field of about 7000 Hz, which was three-fold higher than the maximum frequency generated by our current setup. Two solutions can be envisaged in future work to enhance device performance. First, increasing the pole number of the permanent magnet (although the size and weight of the inductor should be considered so as not to disturb the motor rotation). Second, using a three-fold higher motor speed (e.g., 100 kRPM), which is probably feasible because a few companies have already achieved speeds of approximately 200 kRPM [42]. Many factors are involved in designing and achieving various speeds that now makes these kinds of motors extremely costly. For instance, the expensive dental handpiece is very high speed and can spin at more than 100 kRPM, with some even boasting speeds over 400 kRPM [43]. The highest speed from electrical motors can be achieved by reducing their size to very small and drive negligible loads.

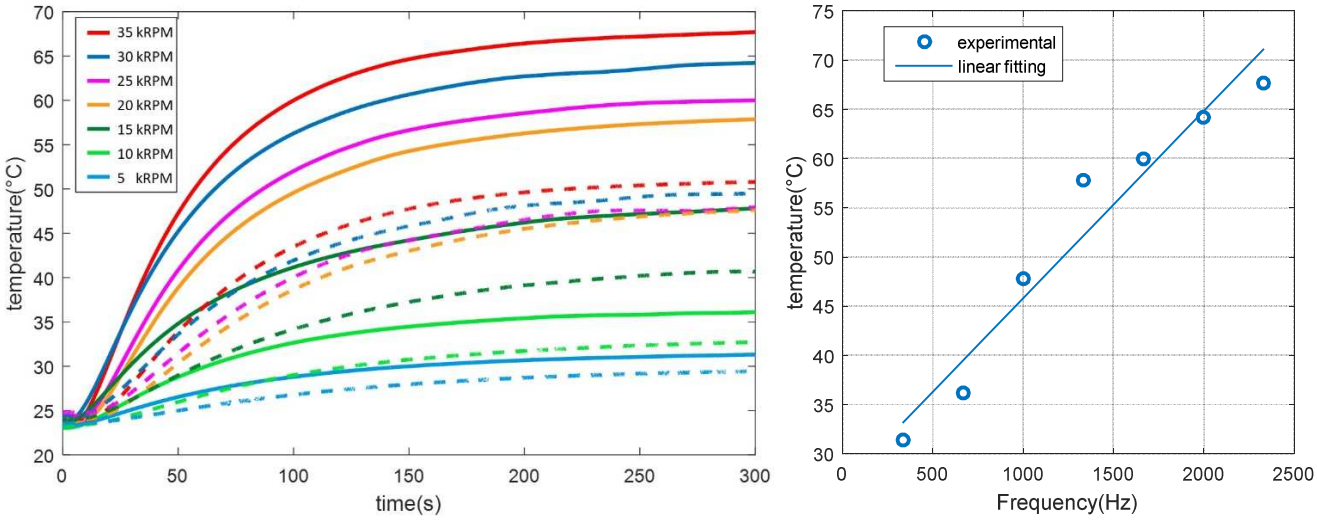

a) b)

Figure 9. a) Temperature versus time at different motor speeds (kRPM). Continuous lines relate to the T° of hot source, whereas dotted lines referred to the T° at the center. b) Temperature versus frequency of alternative magnetic excitation.

The above experiments highlighted the frequency dependence of the induction heating effect and determined how to improve it. It was clear that such an effect also depended on the strength of the magnetic field. To vary the magnetic intensity driven to the sample, it is not necessary to change the permanent magnets. Instead, an easier way was to modify the distance between the magnetic source and the sample. Figure 10a shows the time evolution in temperature for several distances under 2300 Hz magnetic excitation. As expected, the temperature drastically dropped when the distance increased, which was because the strength of the magnetic field decreased quadratically with increasing distance, as described in Figure 10b. Figure 10c illustrates the final temperature in term of the field amplitude, showing how important it is to bring the magnetic source close to the target object.

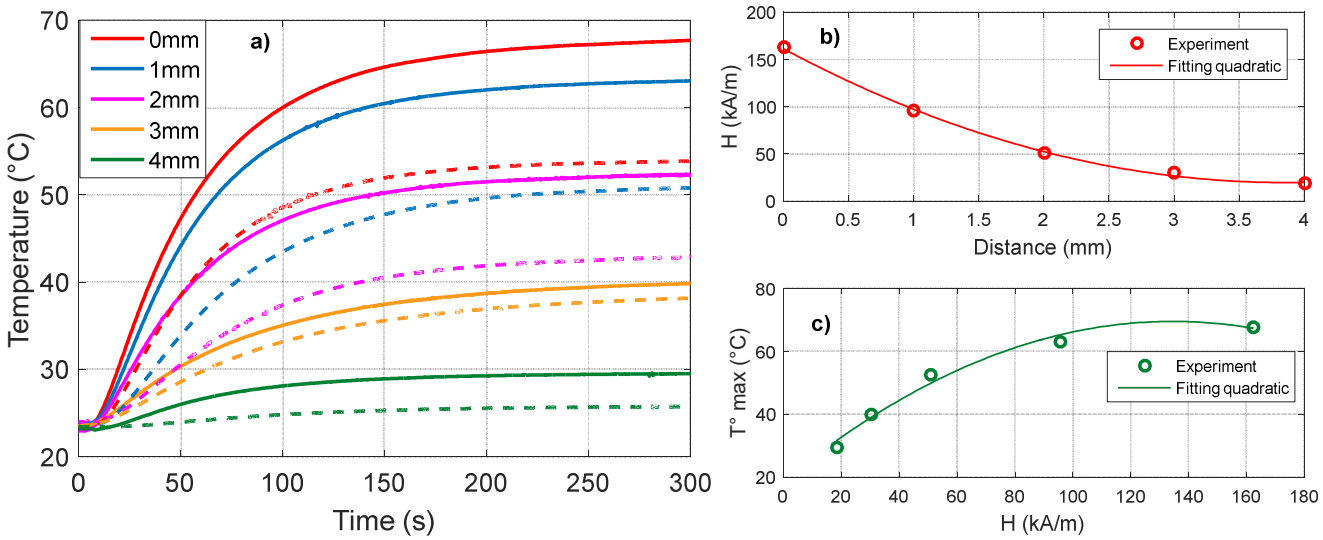

Figure 10. Time evolution of temperature at different distances between the composite and the magnetic inductor. Continuous lines show to the T° of hot source whereas dotted lines show the T° at the center. b) The amplitude of the magnetic field as a function of distance. c) Final temperature versus magnetic intensity.

Accordingly, all previous analyses demonstrated the feasibility to attain a high enough temperature for endovenous thermal ablation that depends on relevant parameters, such as fraction content of fillers, frequency, and strength of the magnetic field. Beside the temperature value, another factor plays a key role in varicose treatment success is the response time of the device, which should not exceed a few seconds in order not to deteriorate the vessel and limit procedure duration. Actually, endovenous procedure obliged that the heating device should deliver an impulsion at maximum amplitude of 120° for less than 5s when treating one segment of varicose vein. In reality, the main limitation of current endovascular therapy is that it cannot heat portion of veins larger than 11 mm for radiofrequency (RFA) and 20 mm for laser (EVLA), leading to increasing treatment time.

Figure 11 displays the evolution of the time constant, where the system has changed about 63% toward its steady-state value. It is noteworthy that the time constant slightly changed as a function of the filler's volume fraction, as well as the frequency and the amplitude of the magnetic field. However, this value is still high relative to the one imposed by treatment of superficial venous insufficiency. A discussion on this issue is presented below.

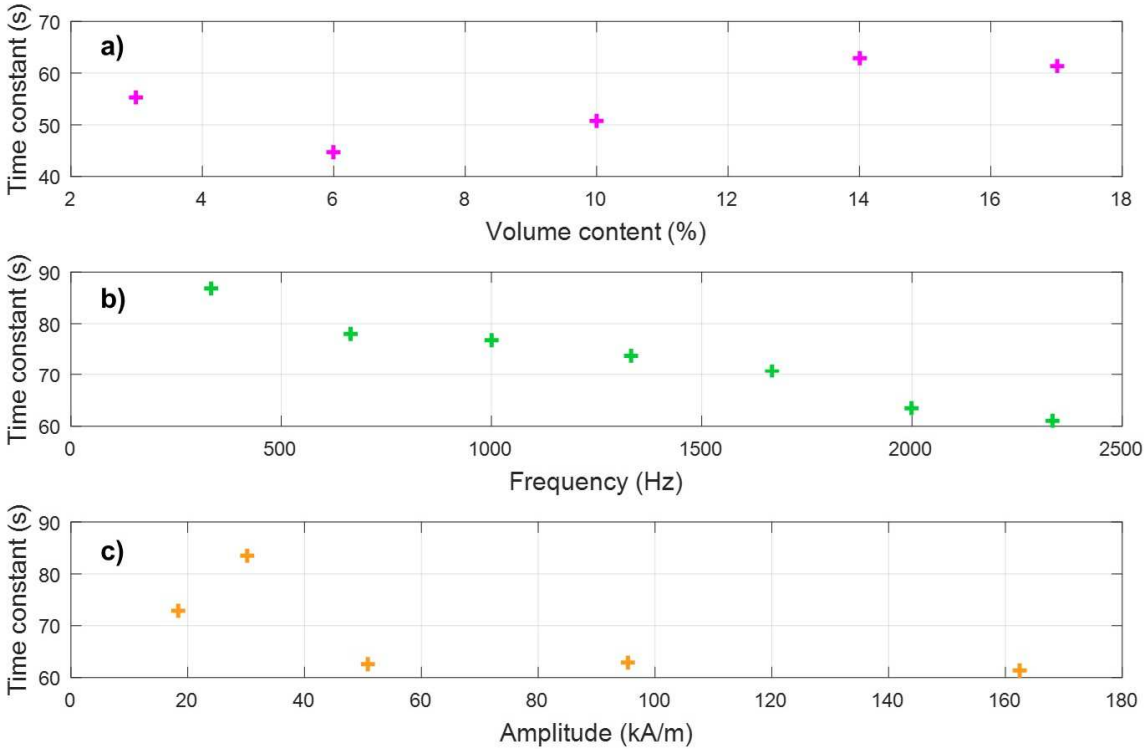

Figure 11. The time constant as a function of a) volume content, b) frequency of magnetic field, and c) amplitude of magnetic field.

IV.3 Analyzing thermal effects based heat transfer modeling

For a deeper analysis of the pertinent parameters affecting the thermal behavior of the ferromagnetic composite, this subsection investigates the finite element modeling-based Comsol Multiphysics simulation. The imaging result from the thermal camera of Figure 6a revealed that the thermal transfer phenomenon could be considered to be symmetric with respect to the center of the sample. In other words, it can be assumed that both sides of the composite were driven by two identical heat sources, as displayed in Figure 12, for the different volume particle contents of 3%, 10%, and 17%. Before investigating each pixel region at a microscopic scale, the whole homogeneous sample with radiation and air convection surfaces were simulated to obtain the average magnetic heating power (MHP) and temperature distribution in the length direction of the sample. The MHP value of the heat source at both sides was estimated by fitting the theoretical average temperature distribution to the experimental temperature measurements at the hottest area of the sample. Indeed, the MHP of the 17% vol. sample was equal to 1.3×10^6 $W.m^{-3}$, which was determined by parameter scanning until the average surface temperature at both sides approximately equals 65°C, as detected by the thermal camera.

The result in Figure 13 highlights the excellent agreement between the theoretical and the empirical temperatures at the center, as well as at the heating zone, achieved for the polymer doped with 17%vol. of iron oxide powder, thus confirming the high reliability of the proposed simulation model together with the calculation of the MHP. A similar behavior was obtained with the 3% and 10% samples.

Table 2 summarizes the setting parameters used for the macroscopic composite model with different volume fractions. The material was supposed to be applied under a magnetic intensity of 160 kA/m at 2300 Hz.

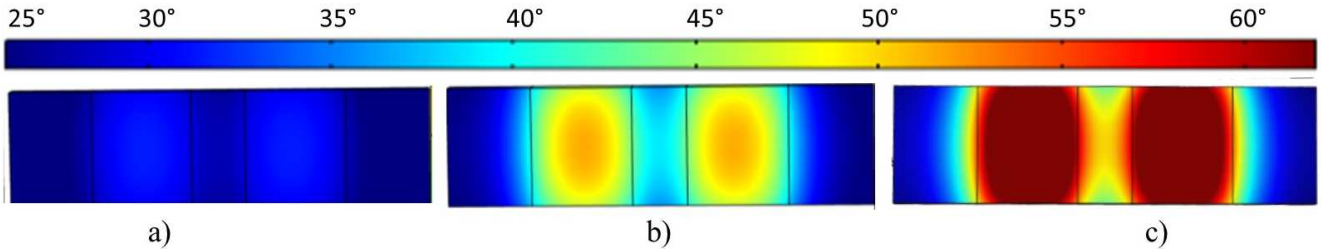

Figure 12. Spatial evolution of temperature for the macroscopic scale of the ferromagnetic composite with a) 3% vol. fraction, c) 10% vol. fraction and c) 17% vol. fraction.

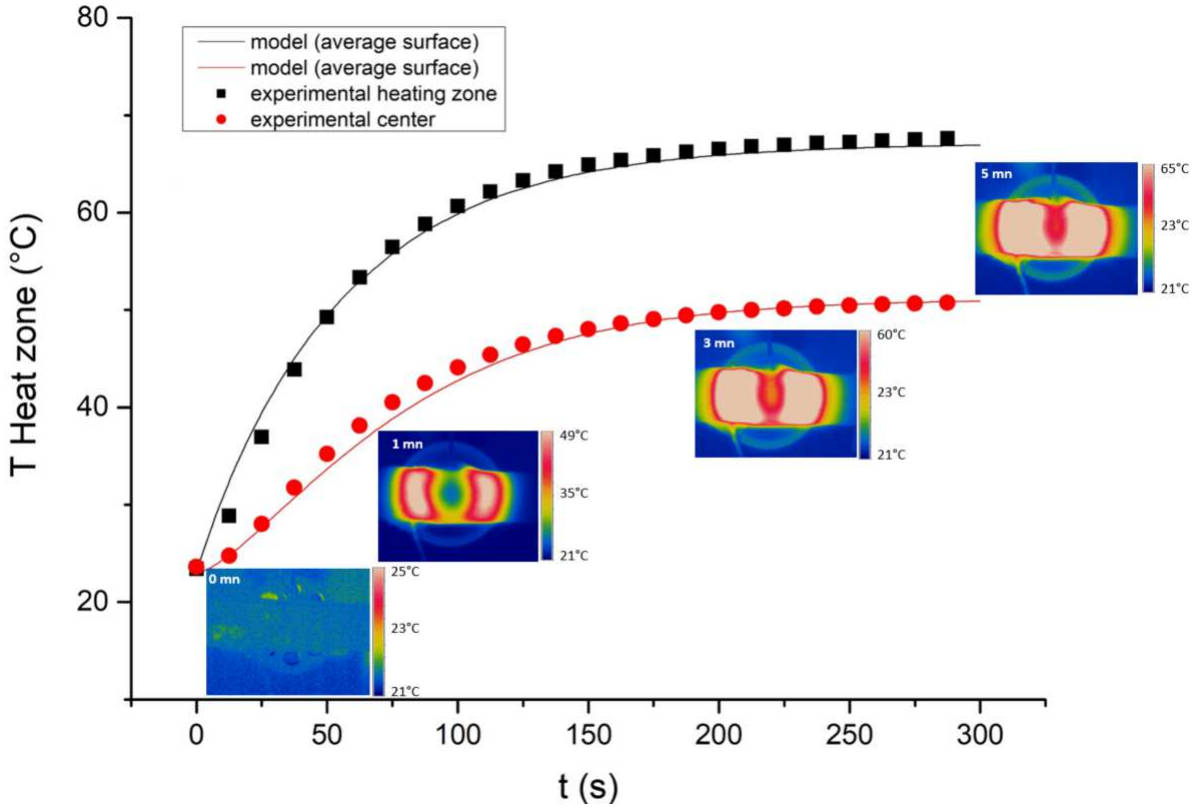

Figure 13. a) Theoretical and experimental temperatures as a function of time for the 17% vol. fraction composite.

Table 2. Simulation thermal parameters of the macroscopic composite model with different contents of the particle.

	3% vol.	**10% vol.**	**17% vol.**
Surface emission ε	0.9	0.9	0.9
Specific heat C_p (J.kg^{-1}.K^{-1})	1260	1040	900
Heat power density P(W.m^{-3})	0.2 x 10^6	0.7 x 10^6	1.3 x 10^6
Thermal conductivity λ (W.m^{-1}.K^{-1})	0.32	0.36	0.4
Transfer coefficient h (W.m^{-2}.K^{-1})	20	20	20

The thermal radiation effect of the surface was taken into account, where the emissivity ε is equivalent to 0.9. The heat transfer coefficient of convection in the air was maintained equal to 20 W.m^{-2}.K^{-1} [44]. As reported in [41], the specific heat capacity (C_p) of a composite below 50% wt. (~ 20% vol.) can be fitted by Eq (6), and is actually equal to the weighted average $C_{p,\ composite}$ of each constituent heat capacities in the case of an isotropic material with constant pressure and volume (negligible thermal expansion) with no local strain or stress [45].

$$C_{p,\,composite} = (1-w)C_{p,ABS} + wC_{p,\,Fe_3O_4} \tag{6}$$

where w denotes the weight concentration of the iron oxide, and $C_{p,ABS}$ and $C_{p,\,Fe_3O_4}$ are the specific heat capacity of the ABS polymer (~ 1600 J.kg^{-1}.K^{-1}) and the Fe_3O_4 particles (~ 450 J.kg^{-1}.K^{-1}) respectively.

Accordingly, the C_p coefficient decreases from 1600 J.kg^{-1}.K^{-1} to 1260, 1040, and 900 J.kg^{-1}.K^{-1} with a magnetic fraction in the polymer at the volume concentrations of 3%, 10%, and 17% respectively.

On the other hand, the thermal conductivity of the composite ($\lambda_{composite}$) tends to enhance when increasing the ferromagnetic content. The Maxwell model is tailored for composites composed of a dispersed and a continuous phase, and gives the following expression for the thermal conductivity in the case of dispersed iron oxide particles in ABS polymer matrix [46]:

$$\lambda_{composite} = \lambda_{ABS} \frac{\lambda_{Fe_3O_4} + 2\lambda_{ABS} + 2x(\lambda_{Fe_3O_4} - \lambda_{ABS})}{\lambda_{Fe_3O_4} + 2\lambda_{ABS} - x(\lambda_{Fe_3O_4} - \lambda_{ABS})} \quad (7)$$

where λ_{p,Fe_3O_4} and λ_{ABS} are the thermal conductivity of the ABS polymer (~ 0.2 W.m^{-1}.K^{-1}) and the Fe_3O_4 particles (~ 3 W.m^{-1}.K^{-1}). According to [47], the thermal conductivity of iron oxide Fe_3O_4 is considered to be constant at a temperature range of 0°–100°C.

To better understanding the induction heating in a microscopic scale, Figure 14 illustrated the thermal transfer of ferromagnetic particles inside a polymer matrix with three different volume fractions of 3%, 10%, and 17%. Assuming that each particle behaved as a heat micro-source with a constant power density (MHP) whose value can be estimated based on the average surface temperature (which was determined previously in the macro model of Figure 12). Consequently, the temperature distribution in the scale of several microns can be mapped by the finite element modeling of thermal transmission and the theoretical estimation of the magnetic heating power. As expected in Figure 14, the sample with high volume fraction (i.e., 17%) possessed a very small inter-particle distance compared to the other, leading to a more regular induction heating effect and thus significantly increasing the temperature of the whole polymer composite. On the other hand, in case of the composite with low magnetic content (i.e., 3%), the inter-particle distance is too important with respect to the particle size, so that thermal transfer among heat sources cannot be assumed to be homogenous, resulting in a decreased global temperature of the entire sample.

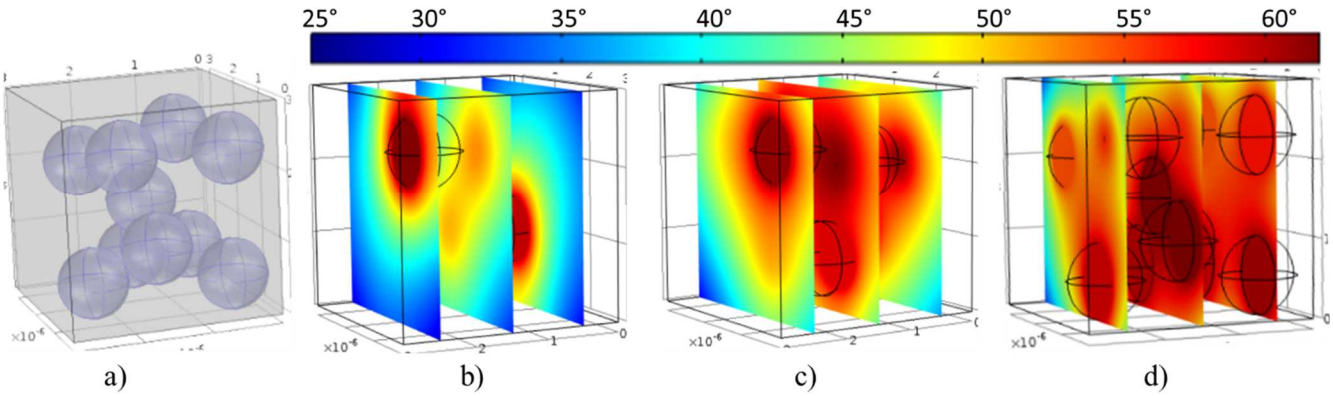

Figure 14. a) Microscopic scale of the ferromagnetic composite. Heat transfer of particles with b) 3% vol. fraction, c) 10% vol. fraction, and d) 17% vol. fraction.

Figure 15a displays the simulating heat power driven by a ferromagnetic particle in a low-frequency excitation. A perfectly linear relationship between the MHP and the frequency was observed, confirming that the energy density corresponding to the hysteresis cycle air of the particle is almost constant (around 20–25 kJ.m^{-3}) in such a frequency range. This simulation result has been used to theoretically draw the hysteresis cycle previously described in subsection III. A similar behavior was also obtained in the case of entire homogenous composite where its MHP value linearly increases as a function of the frequency (Figure 15b).

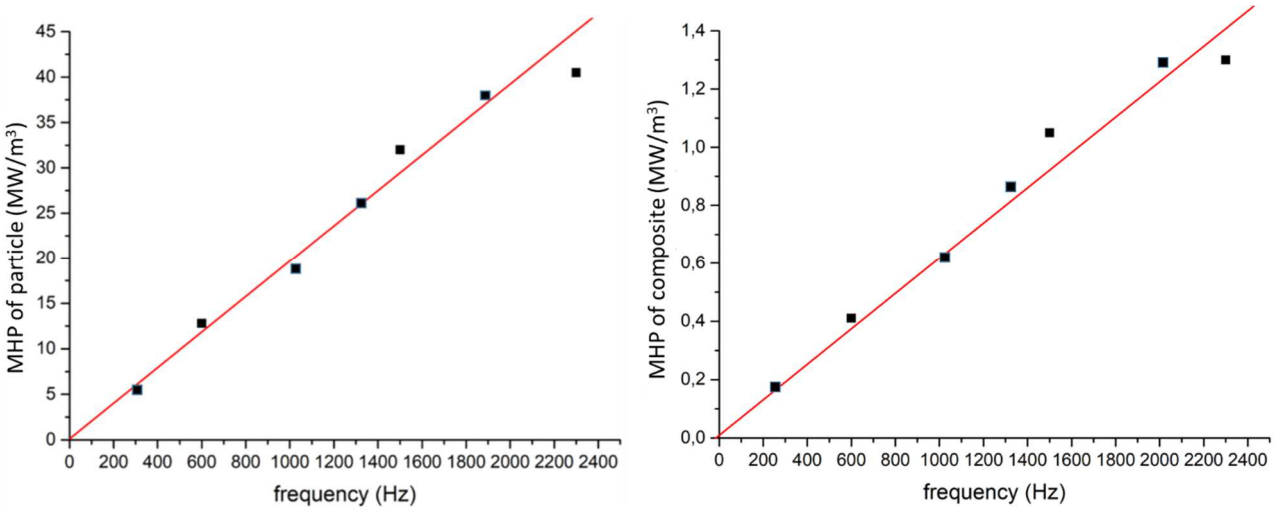

a) b)

Figure 15. Magnetic heat power (MHP) versus frequency a) of Fe_3O_4 particle and b) of composite doped with 17% vol.

So far, with the experiment result of subsection IV.2, it can be concluded that the current setup together with the proposed composite leads to an achievement of maximum temperature around 65° within approximately 3 min. This result confirms the feasibility of inductively heating the composite elaborated with magnetic particles through the use of a rotating magnetic excitation under somewhat low frequency. However, our system performance needed to be dramatically improved to meet the medical requirement for varicose vein operation, where the temperature should rise to 100–120°C for a very short elapse time (usually less than 5 s) to avoid skin burns, hematoma, and nerve injury. Typically, the diameters of varicose veins vary widely due to diversities in individuals, the types of sick veins, and the different location of the human body. Diameters data of varicose veins reported in [48] [49] were collected from the records of several groups of patients. According to these data, we can assume that the maximum varicose veins are about 8 mm. The amount of energy necessary to obliterate the vein was empirically determined by [50], based on previous experience, to be a maximum of 80 J per linear centimeter for a duration not exceeding 4–5 s. Thus, the heating source should generate an average power of about 20 W. According to our simulation result in Figure 15a, the equivalent MHP released by a 17% vol. composite under 2300 Hz frequency was equal to 1.3 W/cm^3. Consequently, to drive enough energy to destroy a 1 cm long vein, the necessary volume of the material is nearly 15 cm^3. This dimension, which is clearly too important compared to the vein's diameter and the incision's size of minimally-invasive procedure, seems to be unrealizable in practice. Another option is to enhance the composite's MHP by increasing its magnetic concentration and/or the alternating frequency of the magnetic source. The following simulation provided a deeper analysis of these relevant parameters that strongly affect the induction heating behavior.

Figure 16a illustrated the time evolution in temperature as a function of volume fraction under 2300 Hz magnetic intensity. Interestingly, the composite doped with 30% vol. concentration allowed us to boost the temperature to close to 100°C, as opposed to our current 17% vol. sample where only 65°C was achieved. Figure 16b shows that the 30% vol. composite gives rise to a final temperature of 220°C at an input magnetic excitation of 7000 Hz, which is higher than the medical need. Obviously, the temperature can be drastically enhanced by increasing the particle concentration and frequency of the magnetic field. However, the filler content of the material should not be above 30–40%vol. to neither exceed the percolation threshold nor favor heterogeneity of the polymer matrix. As mentioned previously in subsection IV.2, the frequency of the magnetic field was controlled by a DC motor whose speed was limited to a few hundred kRPM.

Figure 17a depicted the time evolution of the heating temperature with different sample thicknesses, from 0.2 to 3.2 mm. All composites were supposed to be filled with 30% volume content of iron oxide powdered and were exposed to an alternating magnetic field of 7000 Hz and 160 kA/m amplitude. Interestingly, both final temperature value and its time constant increased as a function of the thickness. After the elapse of three time constants, which corresponds to a 95% change in state, the system is considered to practically achieve its final heating temperature. To get the heating temperature value from 100° to 120° (see Figure 17b), the optimal thickness of the composite should be between 0.7 and 1.2 mm, leading to a response time of about 60 to 90 s (i.e., equivalent to the three-fold time constant). Therefore, by choosing an appropriate sample thickness, as

well as improved fraction content and magnetic source frequency, it is possible to drastically speed up the temperature change, from 3 min (cf. Figure 11) to 1–1.5 min. Other pertinent parameters could affect the heating time constant, and these should be effectively exploited in the next step of this work. For instance, larger volumic masse ρ and larger heat capacity (C_p) lead to slower changes in temperature, while a larger exchange surface area and better heat transfer (h) favors speedily temperature increases. Thereby, to further reduce the time constant to meet medical needs, a possible solution is to use other polymers (thermoplastic or elastomer) with smaller value of specific heat compared to the one of ABS used in this study (~ 1600 $J.kg^{-1}.K^{-1}$), for instance, PMMA with C_p ~ 1270 $J.kg^{-1}.K^{-1}$, or even silicon with extremely low C_p (~ 710 $J.kg^{-1}.K^{-1}$). These polymers may lead to drastically decreased heat capacity of the whole composite, making it possible to enhance the temperature's response time. Another option involves in investigating influence of shape, nature, and size of particles on induction heating behavior so that to obtain the most optimize ferromagnetic material that leads to faster temperature changes. An alternative solution is to increase exchange surface of sample but this solution is not well adapted for medical application where diameter of the heating wire should be sufficiently small to be introduced inside the veins. Finally, a different possible technique is to inductively heat nano-particle materials on very high frequency (HF), around hundreds of kHz at relatively high magnetic strength [51]. This method leads to drastically fast temperature change, of approximately few second for an increase of 100°C, which can match specifications entailed by endovenous procedure [52]. However, the alternative generator used to deliver such high frequency and magnetic amplitude is quite complex and expensive compared to our developed setup where only a DC motor and small permanent magnets were used. Based on very promising experimental and simulation results, we believe that the cost-effective LFIH method can reach requirements endovenous thermal ablation by enhancing the magnetic source as well as optimizing ferromagnetic composite properties. To the best of our knowledge, this is the first time LFIH approach has been demonstrated to be high potential for minimally-invasive therapies. Most recent researches based IH related to medical application (e.g. hyperthermia cancer treatment) requires extremely high power supply up to a few MHz's frequency [53], involving very complex system where accurate power converters and control design become mandatory.

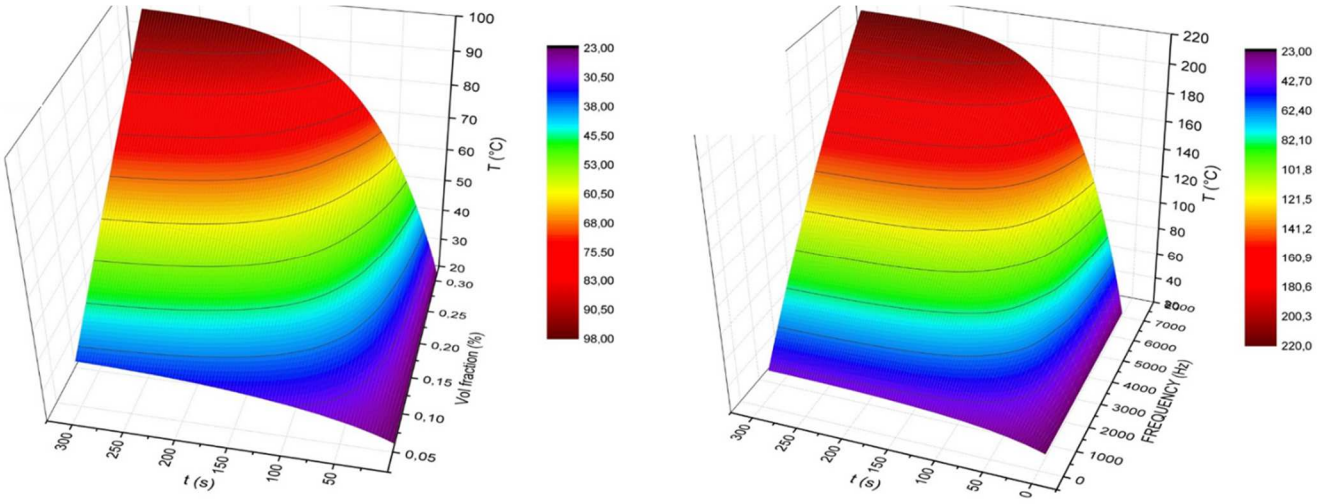

Figure 16. Performance of induction heating in terms of a) volume fraction and b) frequency of the magnetic field.

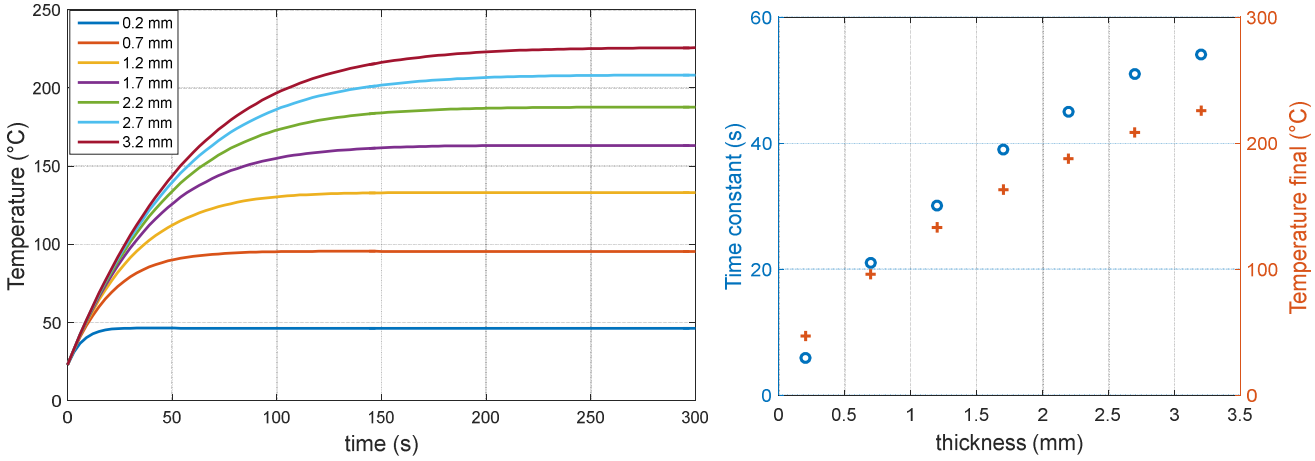

Figure 17. a) Time evolution of temperature with different sample thickness at optimal fraction and frequency of the magnetic field. b) Time constant versus heating temperature for various thickness values.

Finally, further enhancement in terms of experimental setup, as well as material design, should be investigated in future work. This work should aim to meet medical requirements so that varicose veins could be efficiently heated within a very short time.

V CONCLUSIONS

This paper demonstrated the low-frequency induction heating effect on ferromagnetic composites involving ABS thermoplastic polymer filled with iron oxide particles. We found that the heating behavior could be affected by diverse factors, including parameters related to the composites (e.g. content, nature, size of the magnetic particles; dispersion and dimension of composite, homogeneity of the iron powder in the polymer matrix, thermal conductivity and specific heat of both polymer and fillers, etc.), parameters related to the external magnetic excitation (e.g. frequency, amplitude), and parameters related to the external environment (e.g. heat dissipation, thermal exchange). Experimental and simulation results showed the feasibility to inductively heat the ferromagnetic composite to 100–120°C by optimizing the magnetic source and the filler concentration of the material. Another issue regarding the heating speed will be thoroughly investigated to efficiently minimize the time constant (~ few seconds) that was identified as one of the most critical conditions for the minimally-invasive procedure in varicose veins. An alternative aspect of this work focusses on enhancing the mechanical properties of the magnetic composite to be adaptable to additive manufacturing and 3D printing. Finally, the initial experimental results reported in this paper were encouraging, especially for application in thermal endovenous treatments based on the induction heating effect. To confirm the reliability of the proposed approach for real clinical environments, further *in vitro* and *in vivo* tests are under consideration for future research. The next step of this work is to compare the long-term efficacy and the risk-benefit ratio of the LFIH method with those of existing endovenous techniques.

AUTHORS CONTRIBUTION

MQL and BD wrote the manuscript. MQL plotted and analyzed empirical data while BD developed theoretical model. ZX elaborated composites and do all experimental tests. GC gave some advices on fabrication process. PJC developed experimental setup and JFC worked on Comsol simulation. NDS and PL validated the feasibility of the project especially on clinical environment.

REFERENCES

[1] S.H. Huang, P. Liu, A. Mokasdar, L. Hou, Additive manufacturing and its societal impact: A literature review, International Journal of Advanced Manufacturing Technology. 67 (2013) 1191–1203. doi:10.1007/s00170-012-4558-5.

[2] H. Chung, S. Das, Processing and properties of glass bead particulate-filled functionally graded Nylon-11 composites produced by selective laser sintering, Materials Science and Engineering: A. 437 (2006) 226–234. doi:10.1016/j.msea.2006.07.112.

[3] M. Nikzad, S.H. Masood, I. Sbarski, Thermo-mechanical properties of a highly filled polymeric composites for Fused Deposition Modeling, Materials and Design. 32 (2011) 3448–3456. doi:10.1016/j.matdes.2011.01.056.

[4] K. Boparai, R. Singh, H. Singh, Comparison of tribological behaviour for Nylon6-Al-Al2O3 and ABS parts fabricated by fused deposition modelling, Virtual and Physical Prototyping. 10 (2015) 59–66. doi:10.1080/17452759.2015.1037402.

[5] B.J. Knauf, D.P. Webb, C. Liu, P.P. Conway, Low frequency induction heating for the sealing of plastic microfluidic systems, Microfluidics and Nanofluidics. 9 (2010) 243–252. doi:10.1007/s10404-009-0539-x.

[6] B. Ducharne, M.Q. Le, G. Sebald, P.J. Cottinet, D. Guyomar, Y. Hebrard, Characterization and modeling of magnetic domain wall dynamics using reconstituted hysteresis loops from Barkhausen noise, Journal of Magnetism and Magnetic Materials. 432 (2017) 231–238. doi:10.1016/j.jmmm.2017.01.096.

[7] B. Gupta, B. Ducharne, G. Sebald, T. Uchimoto, A Space Discretized Ferromagnetic Model for Non-Destructive Eddy Current Evaluation, IEEE Transactions on Magnetics. 54 (2018) 1–4. doi:10.1109/TMAG.2017.2773517.

[8] M. Arora, Management of varicose veins, JK Science. 19 (2015) 185–189. doi:10.9738/INTSURG-D-14-00084.1.

[9] Renate R., Marianne M.G., Endovenous thermal ablation for varicose veins: strengths and weaknesses, Servier - Phlebolymphology. 19 (2012) 163–169.

[10] M.P. Goldman, Closure of the greater saphenous vein with endoluminal radiofrequency thermal heating of the vein wall in combination with ambulatory phlebectomy: preliminary 6-month follow-up, Dermatol Surg. 26 (2000) 452–456.

[11] J.-J. Liu, L.-H. Fan, D.-C. Xu, X. Li, Z.-H. Dong, W.-G. Fu, The endovenous laser treatment for patients with varicose veins, Pak J Med Sci. 32 (2016) 55–58. doi:10.12669/pjms.321.8610.

[12] Z. Xiang, B. Gupta, M.Q. Le, P.J. Cottinet, B. Ducharne, Hysteresis Model of 3D Printed Magnetic Particles Based Polymer Composite Materials, in: 2018 IEEE International Magnetics Conference (INTERMAG), 2018: pp. 1–5. doi:10.1109/INTMAG.2018.8508119.

[13] D. Grinberg, S. Siddique, M.-Q. Le, R. Liang, J.-F. Capsal, P.-J. Cottinet, 4D Printing based piezoelectric composite for medical applications, Journal of Polymer Science Part B: Polymer Physics. 57 (2019) 109–115. doi:10.1002/polb.24763.

[14] L.H. Rasmussen, M. Lawaetz, L. Bjoern, B. Vennits, A. Blemings, B. Eklof, Randomized clinical trial comparing endovenous laser ablation, radiofrequency ablation, foam sclerotherapy and surgical stripping for great saphenous varicose veins, British Journal of Surgery. 98 (2011) 1079–1087. doi:10.1002/bjs.7555.

[15] T.G. Poder, J.F. Fisette, S.K. Bédard, M.A. Despatis, Is radiofrequency ablation of varicose veins a valuable option? A systematic review of the literature with a cost analysis, Canadian Journal of Surgery. 61 (2018) 128–138. doi:10.1503/cjs.010114.

[16] A.K. Gupta, M. Gupta, Synthesis and surface engineering of iron oxide nanoparticles for biomedical applications, Biomaterials. 26 (2005) 3995–4021. doi:10.1016/j.biomaterials.2004.10.012.

[17] A. Yan, X. Liu, G. Qiu, H. Wu, R. Yi, N. Zhang, J. Xu, Solvothermal synthesis and characterization of size-controlled Fe3O4 nanoparticles, Journal of Alloys and Compounds. 458 (2008) 487–491. doi:10.1016/j.jallcom.2007.04.019.

[18] M.J. Oliveira, A.M. Brito, M.C. Costa, M.F. Costa, Gloss and surface topography of ABS: A study on the influence of the injection molding parameters, Polymer Engineering & Science. 46 (2006) 1394–1401. doi:10.1002/pen.20607.

[19] X. Wang, M. Jiang, Z. Zhou, J. Gou, D. Hui, 3D printing of polymer matrix composites: A review and prospective, Composites Part B: Engineering. 110 (2017) 442–458. doi:10.1016/j.compositesb.2016.11.034.

[20] H. Iida, K. Takayanagi, T. Nakanishi, T. Osaka, Synthesis of Fe3O4 nanoparticles with various sizes and magnetic properties by controlled hydrolysis, Journal of Colloid and Interface Science. 314 (2007) 274–280. doi:10.1016/j.jcis.2007.05.047.

[21] G. Li, Y. Jiang, K. Huang, P. Ding, J. Chen, Preparation and properties of magnetic Fe3O4–chitosan nanoparticles, Journal of Alloys and Compounds. 466 (2008) 451–456. doi:10.1016/j.jallcom.2007.11.100.

[22] Y. Yao, S. Miao, S. Liu, L.P. Ma, H. Sun, S. Wang, Synthesis, characterization, and adsorption properties of magnetic Fe3O4@graphene nanocomposite, Chemical Engineering Journal. 184 (2012) 326–332. doi:10.1016/j.cej.2011.12.017.

[23] D. Caruntu, G. Caruntu, C.J. O\textquotesingleConnor, Magnetic properties of variable-sized Fe3O4nanoparticles synthesized from non-aqueous homogeneous solutions of polyols, J. Phys. D: Appl. Phys. 40 (2007) 5801–5809. doi:10.1088/0022-3727/40/19/001.

[24] M. Mehrmohammadi, K.Y. Yoon, M. Qu, K.P. Johnston, S.Y. Emelianov, Enhanced pulsed magneto-motive ultrasound imaging using superparamagnetic nanoclusters, Nanotechnology. 22 (2011) 045502. doi:10.1088/0957-4484/22/4/045502.

[25] G. Bertotti, I.D. Mayergoyz, The Science of Hysteresis: Hysteresis in materials, Gulf Professional Publishing, 2006.

[26] D.C. Jiles, D.L. Atherton, Theory of ferromagnetic hysteresis, Journal of Magnetism and Magnetic Materials. 61 (1986) 48–60. doi:10.1016/0304-8853(86)90066-1.

[27] B. Zhang, B. Gupta, B. Ducharne, G. Sebald, T. Uchimoto, Preisach's Model Extended With Dynamic Fractional Derivation Contribution, IEEE Transactions on Magnetics. 54 (2018) 1–4. doi:10.1109/TMAG.2017.2759421.

[28] E. Della Torre, Hysteresis modeling, COMPEL. 17 (1998) 682–689. doi:10.1108/03321649810221152.

[29] B. Zhang, B. Gupta, B. Ducharne, G. Sébald, T. Uchimoto, Dynamic Magnetic Scalar Hysteresis Lump Model Based on Jiles–Atherton Quasi-Static Hysteresis Model Extended With Dynamic Fractional Derivative Contribution, IEEE Transactions on Magnetics. 54 (2018) 1–5. doi:10.1109/TMAG.2018.2832242.

[30] D.C. Jiles, A self consistent generalized model for the calculation of minor loop excursions in the theory of hysteresis, IEEE Transactions on Magnetics. 28 (1992) 2602–2604. doi:10.1109/20.179570.

[31] M.A. Raulet, B. Ducharne, J.P. Masson, G. Bayada, The magnetic field diffusion equation including dynamic hysteresis: a linear formulation of the problem, IEEE Transactions on Magnetics. 40 (2004) 872–875. doi:10.1109/TMAG.2004.824816.

[32] B. Ducharne, G. Sebald, D. Guyomar, G. Litak, Dynamics of magnetic field penetration into soft ferromagnets, Journal of Applied Physics. 117 (2015) 243907. doi:10.1063/1.4923162.

[33] B. Ducharne, G. Sebald, D. Guyomar, G. Litak, Fractional model of magnetic field penetration into a toroidal soft ferromagnetic sample, Int. J. Dynam. Control. 6 (2018) 89–96. doi:10.1007/s40435-017-0303-0.

[34] P. Tenant, J.J. Rousseau, Dynamic model of magnetic materials applied on soft ferrites, IEEE Transactions on Power Electronics. 13 (1998) 372–379. doi:10.1109/63.662859.

[35] Methods of measurement of the magnetic properties of magnetically soft metallic and powder materials at frequencies in the range 20hz to 200khz by the use of ring specimens, (2003).

[36] Methods of measurement of the magnetic properties of electrical steel strip and sheet by means of an Epstein frame, (2008).

[37] Test method for alternating-current magnetic properties of materials at power frequencies using wattmeter-ammeter-voltmeter method and 25-cm Epstein test frame, (2008).

[38] Methods of measurement of the magnetic properties of electrical steel strip and sheet by means of a single sheet tester, (2002).

[39] Guide for measuring power frequency magnetic properties of flat-rolled electrical steels using small single sheet testers, (2009).

[40] T. Bayerl, R. Schledjewski, P. Mitschang, Induction heating of thermoplastic materials by particulate heating promoters, Polymers and Polymer Composites. 20 (2012) 333–342.

[41] L. Riviere, N. Causse, A. Lonjon, E. Dantras, C. Lacabanne, Specific heat capacity and thermal conductivity of PEEK/Ag nanoparticles composites determined by Modulated-Temperature Differential Scanning Calorimetry, Polymer Degradation and Stability. 127 (2016) 98–104.

[42] P. Pfister, Y. Perriard, Very-High-Speed Slotless Permanent-Magnet Motors: Analytical Modeling, Optimization, Design, and Torque Measurement Methods, IEEE Transactions on Industrial Electronics. 57 (2010) 296–303. doi:10.1109/TIE.2009.2027919.

[43] Side-by-side comparison of High-Speed Dental Handpiece Attachments | Dentalcompare.com, (n.d.). https://www.dentalcompare.com/Restorative-Dentistry/5149-Dental-Handpiece-Attachments/Compare/?compare=34229,3132945,3132954,3082130&catid=5149 (accessed March 4, 2019).

[44] Y. Yang, J. He, Q. Li, L. Gao, J. Hu, R. Zeng, J. Qin, S.X. Wang, Q. Wang, Self-healing of electrical damage in polymers using superparamagnetic nanoparticles, Nature Nanotechnology. 14 (2019) 151. doi:10.1038/s41565-018-0327-4.

[45] B. Budiansky, Thermal and thermoelastic properties of isotropic composites, Journal of Composite Materials. 4 (1970) 286–295.

[46] J. Wang, J.K. Carson, M.F. North, D.J. Cleland, A new structural model of effective thermal conductivity for heterogeneous materials with co-continuous phases, 51 (2008) 2389–2397. doi:10.1016/j.ijheatmasstransfer.2007.08.028.

[47] S. Ramirez, K. Chan, R. Hernandez, E. Recinos, E. Hernandez, R. Salgado, A.G. Khitun, J.E. Garay, A.A. Balandin, Thermal and magnetic properties of nanostructured densified ferrimagnetic composites with graphene - graphite fillers, Materials & Design. 118 (2017) 75–80. doi:10.1016/j.matdes.2017.01.018.

[48] K. Gibson, M. Meissner, D. Wright, Great saphenous vein diameter does not correlate with worsening quality of life scores in patients with great saphenous vein incompetence, Journal of Vascular Surgery. 56 (2012) 1634–1641. doi:10.1016/j.jvs.2012.02.065.

[49] A. Yasim, E. Eroglu, O. Bozoglan, B. Mese, M. Acipayam, H. Kara, A new non-tumescent endovenous ablation method for varicose vein treatment: Early results of N-butyl cyanoacrylate (VariClose®), Phlebology. 32 (2017) 194–199. doi:10.1177/0268355516638577.

[50] L.M.A. Viarengo, J. Potério-Filho, G.M.B. Potério, F.H. Menezes, G.V. Meirelles, Endovenous laser treatment for varicose veins in patients with active ulcers: Measurement of intravenous and perivenous temperatures during the procedure, Dermatologic Surgery. 33 (2007) 1234–1241. doi:10.1111/j.1524-4725.2007.33259.x.

[51] O. Lucía, P. Maussion, E.J. Dede, J.M. Burdío, Induction Heating Technology and Its Applications: Past Developments, Current Technology, and Future Challenges, IEEE Transactions on Industrial Electronics. 61 (2014) 2509–2520. doi:10.1109/TIE.2013.2281162.

[52] N. Hohlbein, A. Shaaban, A.M. Schmidt, Remote-controlled activation of self-healing behavior in magneto-responsive ionomeric composites, Polymer. 69 (2015) 301–309. doi:10.1016/j.polymer.2015.04.024.

[53] P.R. Stauffer, T.C. Cetas, R.C. Jones, Magnetic Induction Heating of Ferromagnetic Implants for Inducing Localized Hyperthermia in Deep-Seated Tumors, IEEE Transactions on Biomedical Engineering. BME-31 (1984) 235–251. doi:10.1109/TBME.1984.325334.

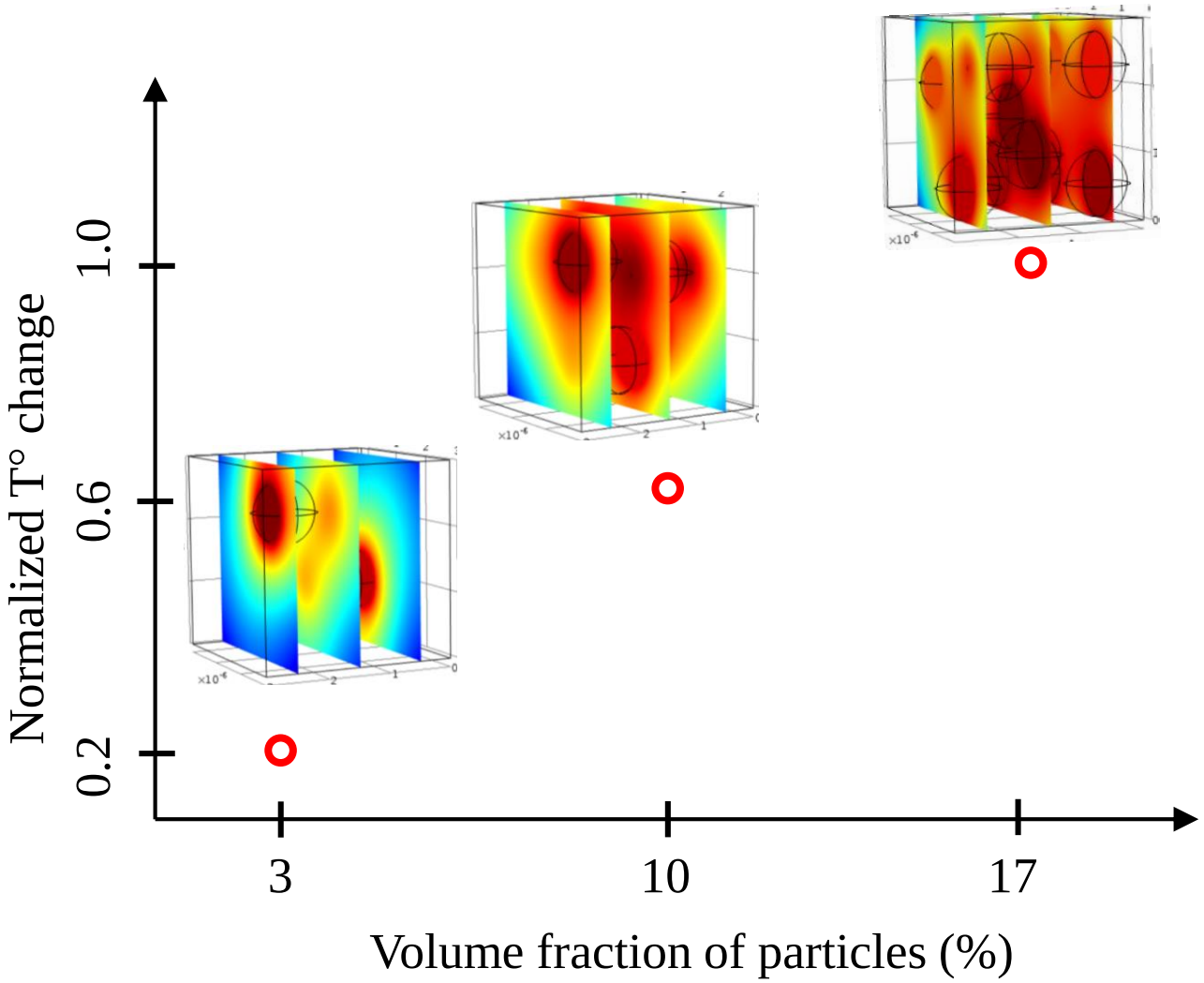
Normalized T° change
1.0
0.6
0.2
3
10
17
Volume fraction of particles (%)

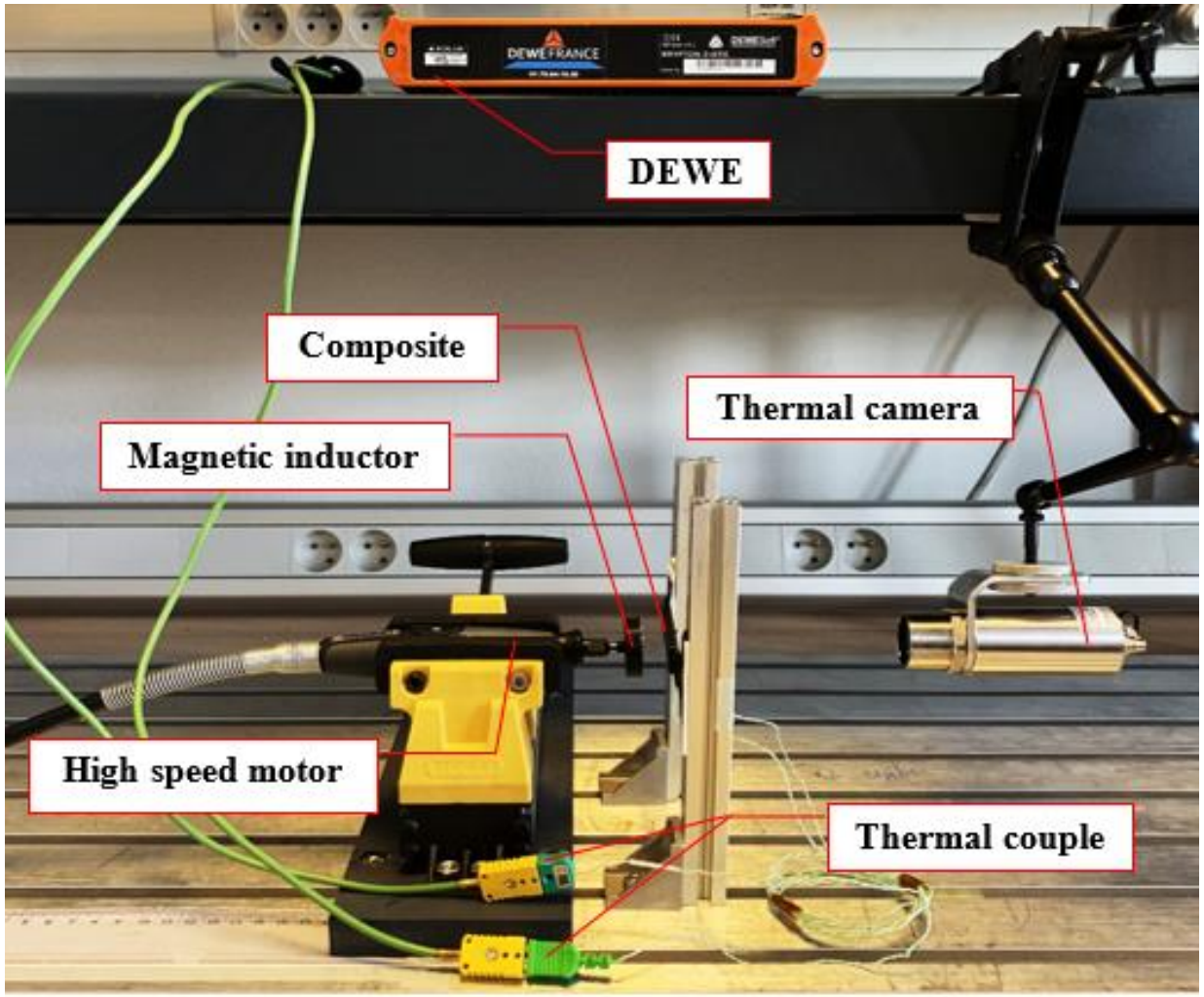
DEWE
Composite
Thermal camera
Magnetic inductor
High speed motor
Thermal couple